Frontiers in Bioscience Landmark

Front. Biosci. (Landmark Ed) **2025**; 30(1): 26721
https://doi.org/10.31083/FBL26721

Original Research

Atomized Neutrophil Membrane-coated MOF Nanoparticles for Direct Delivery of Dexamethasone for Severe Pneumonia

Yixiao Yang[1,2,†], Lizhen Yan[3,†], Han Zhang[1,4], Chuanguang Xiao[5,*], Kai Wang[1,*]

[1]Institute of Translational Medicine, Shanghai University, 200444 Shanghai, China
[2]Institute of Burn Research, The First Affiliated Hospital, State Key Lab of Trauma, Burn and Combined Injury, Chongqing Key Laboratory for Disease Proteomics, Third Military Medical University (Army Medical University), 400038 Chongqing, China
[3]Department of Respiratory and Critical Care Medicine, Zibo Municipal Hospital, 255400 Zibo, Shandong, China
[4]MPA Key Laboratory for Research and Evaluation of Tissue Engineering Technology Products, Medical College, Nantong University, 226001 Nantong, Jiangsu, China
[5]Department of Breast Thyroid Surgery, Zibo Central Hospital, 255036 Zibo, Shandong, China
*Correspondence: sdxiaochuanguang@163.com (Chuanguang Xiao); kaiwang16@fudan.edu.cn (Kai Wang)
[†]These authors contributed equally.
Academic Editor: Hongwei Yao
Submitted: 24 September 2024 Revised: 26 November 2024 Accepted: 29 November 2024 Published: 22 January 2025

Abstract

Background: Dexamethasone has proven life-saving in severe acute respiratory syndrome (SARS) and COVID-19 cases. However, its systemic administration is accompanied by serious side effects. Inhalation delivery of dexamethasone (Dex) faces challenges such as low lung deposition, brief residence in the respiratory tract, and the pulmonary mucus barrier, limiting its clinical use. Neutrophil cell membrane-derived nanovesicles, with their ability to specifically target hyper-activated immune cells and excellent mucus permeability, emerge as a promising carrier for pulmonary inhalation therapy. **Methods**: We designed a novel UiO66 metal-organic framework nanoparticle loaded with Dex and coated with neutrophil cell membranes (UiO66-Dex@NMP) for targeted therapy of severe pneumonia. This was achieved by loading Dex into UiO66 pores and subsequently coating with neutrophil membranes for functionalization. **Results**: Drug release experiments revealed UiO66-Dex@NMP to exhibit favorable sustained-release properties. Additionally, UiO66-Dex@NMP demonstrated excellent targeting capabilities both *in vitro* and *in vivo*. In a mouse model of lipopolysaccharide (LPS)-induced pneumonia, UiO66-Dex@NMP significantly reduced lung inflammation compared to both the control model and Dex administered via inhalation. Histopathological analysis further confirmed UiO66-Dex@NMP's ability to alleviate lung tissue damage. **Conclusions**: UiO66-Dex@NMP represents a novel and safe inhaled delivery carrier for Dex, offering valuable insights into the clinical management of respiratory diseases, including severe pneumonia.

Keywords: dexamethasone; MOF; neutrophil cell membrane; inhaled delivery; severe pneumonia

1. Introduction

Severe pneumonia (SP) is a major respiratory disease and a leading cause of death among children and the elder [1–3]. SP can be caused by infections from various pathogens, including bacteria, viruses, fungi, mycoplasma, and chlamydia. Among these, bacterial and viral infections are the two most common causes [4,5]. The COVID-19 virus, in particular, has been associated with severe lung injury and fatality [6]. Macrophage dysfunction plays a pivotal role in the pathogenesis of severe lung injury, including their involvement in cytokine storms [7,8]. Consequently, the regulation of macrophage activity is of utmost importance. Dexamethasone (Dex) has emerged as the first and most effective drug in saving the lives of patients requiring invasive mechanical ventilation [9]. The glucocorticoid receptor, which is the receptor for dexamethasone, is widely expressed in various cells throughout the body [10]. Due to this high expression, dexamethasone has significant side effects and should be used with caution in clinical settings. Dex exhibits significant side effects and is therefore used with caution in clinical practice. Both oral and intravenous formulations lack pulmonary targeting, leading to systemic toxicity [11]. Nebulized administration represents an ideal method for local delivery. In clinical practice, Dex is commonly administered as dexamethasone sodium phosphate. While inhaled preparations have effectively addressed the issue of pulmonary targeting, they still need to overcome the pulmonary mucus barrier. Furthermore, the deposition rate of nebulized dexamethasone sodium phosphate in the lungs is low, and its residence time in the respiratory tract is brief. Hence, optimizing dosage forms is essential to address these challenges.

Biomimetic functionalized materials provide a new method for the targeting treatment [12,13]. Recent advances in cell membrane mediated drug delivery may help to improve SP treatment efficacy by targeting the potent corticosteroid drug to hyper-activated immune cells [14], offering many new opportunities to push the limit of current therapeutics [15,16]. Neutrophils can typically rush to inflammatory sites within the body, eliminate pathogens,

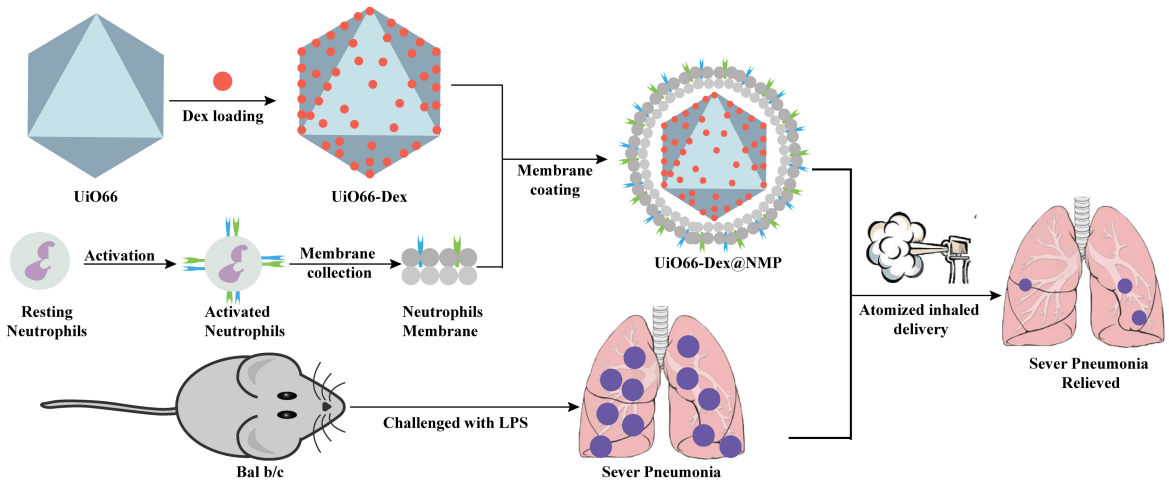

Fig. 1. Schematic illustration of UiO66-Dex@NMP and animal experiment process. LPS, lipopolysaccharide; UiO66-Dex@NMP, UiO66 Metal-Organic Frameworks nanoparticle loaded with dexamethasone (Dex) and coated with neutrophil cell membranes.

and ultimately be cleared by macrophages [17,18]. The targeting ability of neutrophils is facilitated by the interaction of adhesion molecules and integrins, enabling precise delivery of anti-inflammatory drugs to hyper-activated macrophages.

Metal-Organic Frameworks (MOF) are formed through the coordination bonding of metal ions and organic ligands, resulting in a highly ordered porous structure with a large surface area, thus exhibiting excellent adsorption properties [19,20]. In terms of drug delivery, embedding drug molecules into the pores of MOF materials enables controlled release and targeted delivery of drugs [21]. This controlled release mechanism helps to improve the therapeutic effect of drugs while reducing side effects. MOFs have been reported as a viable option for nebulization therapy in the throat due to the effective deposition of micrometer-sized MOF particles within the throat region [22]. Given the limitations of existing respiratory inhalation carriers, there is significant value in developing novel MOF-based pulmonary drug delivery carriers.

In this study, we prepared Dex-loaded UiO66 (UiO66-Dex), subsequently, the surface was coated with neutrophil membranes. UiO66 Metal-Organic Frameworks nanoparticle loaded with dexamethasone (Dex) and coated with neutrophil cell membranes (UiO66-Dex@NMP) was explored inhalation therapy in mice model of lipopolysaccharide (LPS) induced pneumonia (Fig. 1). We anticipate to improve the dosage form and administration of Dex in combination with the current clinical needs.

2. Materials and Methods

2.1 Reagent Materials

Benzene-1,4-dicarboxylic acid (BDC), Zirconium (IV) oxide chloride octahydrate ($ZrOCl_2 \cdot 8H_2O$), N,N-dimethylformamide (DMF) and lipopolysaccharides from Escherichia coli O111:B4 (LPS) were purchased from Sigma-Aldrich (Saint Louis, MO, USA). Percoll and erythrocyte lysate were purchased from Solarbio Biotechnology (Beijing, China). The BCA protein assay kit, Cell Membrane Green Fluorescence Staining Kit (DiO), EISA kits for mouse tumor necrosis factor-α (TNF-α) (P5318, Beyotime, Shanghai, China) and inflammatory factors interleukin 6 (IL-6) (PI335, Beyotime, Shanghai, China) were purchased from Shanghai Beyotime Biotechnology (Shanghai, China). MTT kit was purchased from Shanghai Jiji Biochemical Technology (Shanghai, China).

2.2 Cells and Animals

RAW264.7 cells and DMEM were purchased from Shanghai FuHeng Biology Co., Ltd. (Shanghai, China). All cell lines were validated by short tandem repeat (STR) profiling and tested negative for mycoplasma. Culture conditions: gas phase: 95% air, 5% carbon dioxide. Temperature: 37 °C, incubator humidity maintained at 70%–80%. Cryoprotectant solution: 90% fetal bovine serum (FBS) (C0226, Beyotime, Shanghai, China), 10% DMSO, prepared fresh and used immediately. Healthy, 8-week-old, male BALB/c mice of SPF (Specific Pathogen Free) grade were purchased from Cavens Laboratory Animal Co., Ltd. (Changzhou, Jiangsu, China). All mice weighed between 20 and 25 grams. The animal experiment was approved under approval number AMUWEC20210417, and all procedures were conducted in strict compliance with the relevant regulations and guidelines set by the Laboratory Animal Welfare and Ethics Committee of Third Military Medical University.

2.3 Neutrophil and Neutrophil Membrane Collection

After being anesthetized with 100% carbon dioxide for five minutes, the BALB/c mouse underwent euthanasia to ensure complete cessation of life. After the euthanasia of the BALB/c mouse, the femur and tibia were surgi-

cally removed. Subsequently, the bone ends were neatly trimmed, and an RPMI 1640 solution, enriched with 10% FBS and 2 mM ethylene diamine tetraacetic acid (EDTA), was aspirated to flush out the bone marrow cells. To lyse the red blood cells, 20 mL of a 1.6% NaCl solution was added. Utilizing Percoll in combination with density gradient separation techniques, neutrophils were successfully purified from the bone marrow cells. To identify the purified neutrophils and for downstream experimental purposes, flow cytometry was performed. Additionally, the isolated neutrophils were stained with Shanghai Beyotime Biotechnology Wright-Giemsa kit (C0131, Shanghai, China) and examined under a microscope.

In order to obtain the neutrophil membrane, the neutrophils were destroyed with a low osmotic dissolution buffer containing protease inhibitors for 20 minutes. BeyoZonase broad spectrum nucleases (D7121, Shanghai, China) were added to the solution and treated for 10 minutes. The cells were immersed in liquid nitrogen and 37 ℃ water baths for 5 consecutive cycles of cell destruction. After centrifugation at 1000 g for 5 minutes, the precipitate was discarded. The enriched supernatant was centrifuged at 20,000 g for 30 minutes and 80,000 g for 1.5 hours, respectively. The precipitate was collected and washed three times with PBS mixed with protease inhibitors. Under low temperature conditions, ultrasound was used to obtain dispersed cell membranes.

2.4 Preparation of UiO66 Nanoparticles

The method used in the reference literature employs solvothermal synthesis to prepare UiO66 nanoparticles. The specific steps are as follows: 200 mg of benzene-1,4-dicarboxylic acid (BDC) and dissolve it in 2 mL of N,N-dimethylformamide (DMF). Add the solution to a round-bottom flask and stir for more than 5 minutes. Then, weigh 42 mg of zirconium oxychloride octahydrate ($ZrOCl_2 \cdot 8H_2O$) and dissolve it in 6 mL of DMF. Add the 6 mL of DMF containing zirconium oxychloride octahydrate to the above solution and mix the two solutions for 5 minutes. Afterward, add 4 mL of acetic acid. Seal the round-bottom flask containing the mixed solution and place it in an oil bath at 110 °C. Stir and react for 5 hours. Afterward, centrifuge the obtained product and wash it twice with DMF and deionized water, respectively. Dry the product overnight under vacuum and calculate the yield.

2.5 Preparation and Characterization of UiO66-Dex

The particle size, potential of the samples were detected by Malvern laser particle sizer (NS-90, Malvern, Malvern, UK). Mix 20 mg Dex with 100 mg UiO66, disperse in 20 mL anhydrous ethanol, and stir overnight at room temperature. Then centrifuge the mixture at a speed of 80,000 rpm for 10 minutes, collect the supernatant, and resuspend the precipitate with anhydrous ethanol. Continue centrifugation three times, collecting each supernatant. The morphology of the prepared sample was examined using a transmission electron microscope (TEM) (HT7700, Hitachi, Japan). Quantify the content of free Dex in the supernatant using high performance liquid chromatography (HPLC) (HPLC 1260, Agilent, Santa Clara, CA, USA) and record it as WF. Then, the obtained precipitate was vacuum dried at 120 °C for 24 hours to obtain UiO66-Dex, whose weight was recorded as WNP. Determination of drug loading content and encapsulation efficiency. The encapsulation efficiency and loading content of Dex were calculated as follows:

$$\text{Drug Loading content} = (\text{WT} - \text{WF})/\text{WNP} \times 100\% \quad (1)$$

where WT is the total weight of Dex fed, WF is the weight of non-encapsulated free Dex, and WNP is the weight of nanoparticles.

$$\text{Drug Encapsulation efficiency} = (\text{WT} - \text{WF})/\text{WT} \times 100\% \quad (2)$$

where WT is the total weight of Dex fed, and WF is the weight of non-encapsulated free Dex.

2.6 Preparation and Characterization of Neutrophil Membrane-coated UiO66-Dex@NMP

The neutrophil membrane proteins were determined by a BCA protein assay kit and adjusted to 5 mg/mL. Subsequently, they were mixed with UiO66-Dex (1 mg/mL) in a volume ratio of 1:1. The above mixture was ultrasonically mixed under low-temperature conditions and then passed through an Avant extruder (Avanti Polar Lipids, Inc.,610000, Alabaster, AL, USA) to coat the neutrophil membrane on the surface of UiO66-Dex. The morphology of the prepared sample was examined using a transmission electron microscope (HT7700, Hitachi, Japan).

2.7 Drug Loading and Release

To investigate the release of UiO66-Dex@NMP, a dialysis method was employed. Briefly, UiO66-Dex@NMP loaded with 100 μg of Dex was placed into a dialysis bag with a molecular weight cutoff of 3 kDa. The dialysis bag was then immersed in 20 mL of PBS and incubated at 37 °C for various durations while continuously shaking at 100 rpm. At designated time points, 1 mL of the external medium was removed and replaced with the same volume of PBS. The concentration of Dex released into the bulk dialysis medium was determined by high performance liquid chromatography (HPLC).

2.8 Cytotoxicity

RAW264.7 cells were added to 96-well plates at 1×10^5 cells/well and incubated for 24 hours. Dex, UiO66, UiO66-Dex@NMP solutions at 10, 50, 100, 200, and 500 μg/mL were added into the incubator. After incubation for

48 hours, 20 µL of MTT reagent was added to each well and incubation was continued for 4 hours. 200 µL of DMSO was added to dissolve metazan. Absorbance was measured with an enzyme meter (BioTek ELx808, Winooski, VT, USA).

2.9 Effect of UiO66-Dex@NMP on Cellular Secretion of Inflammatory Factors

RAW264.7 cells were added into 96-well plates at 1 $\times$ 10^5 cells/well, and put into the incubator for 24 hours. The wells were divided into Control, SP+PBS, SP+Dex and SP+UiO66-Dex@NMP groups, in which cells were stimulated with viruses except for the Control group, and then different drugs were added respectively, and put into the incubator for 12 hours. Cells were incubated with enzyme-labeled antibody working solution for 3 hours, and then added termination solution for 20 minutes, and the optical density (OD) value was determined by enzyme marker. The levels of inflammatory factors TNF-α, IL-6, IL-10 were detected according to the instructions of each kit.

2.10 In Vitro Targeting Study

Firstly, UiO66-Dex@NMP was incubated with a cell membrane green fluorescence staining kit for 10 minutes. After centrifugation to wash away excess fluorescent dye, DiO-labeled UiO66-Dex@NMP was resuspended in physiological saline solution. RAW264.7 cells were seeded in a confocal dish at a concentration of 1 $\times$ 10^5/mL and cultured overnight in a cell incubator at 37 °C with 5% CO_2. LPS was added to the RAW264.7 cells at a final concentration of 100 ng/mL, and the cells were further cultured for 2 hours. The culture medium was aspirated, and the cells were washed twice with PBS before replacing it with DMEM medium. After another 4 hours of culture, DiO-labeled UiO66-Dex@NMP was added, and the cells were incubated for another 2 hours. The culture medium was aspirated again, and the cells were washed three times with PBS. Subsequently, the cells were fixed with 4% paraformaldehyde for 15 minutes, washed twice with PBS, and observed under a confocal microscope (LSM800, Zeiss, Germany) to assess the internalization of UiO66-Dex@NMP by the cells.

2.11 Establishment of SP Mouse Model

The animals were situated in a controlled environment with a consistent 12-hour light-dark cycle, allowing them unrestricted access to standard food and water. Subsequently, the mice were gently anesthetized with isoflurane before being intranasally administered 35 µL LPS solution (20 mg/mL) to induce a pneumonia model.

2.12 In Vivo Biodistribution Study

First, UiO66-Dex@NMP was incubated with the DiR fluorescence staining kit for 10 minutes. After that, it was centrifuged and washed three times, and then adjusted to an appropriate concentration with physiological saline. Next, the mice with pneumonia were anesthetized and inhaled the commercially available aerosolized UiO66-Dex@NMP labeled with DiR (MB12482, MeiluneBio, Dalian, Liaoning, China). Four hours after the atomized treatment, the distribution of UiO66-Dex@NMP within the body was examined using a small animal *in vivo* imaging system (IVIS Spectrum, Perkin Elmer, Waltham, MA, USA).

2.13 In Vivo Therapy of SP Mouse Model

The SP model mice were established through induction as described in 2.11. SP model mice were randomly assigned to four groups, each containing five animals: the normal control group, the SP model control group, the Dex treatment group, and the UiO66-Dex@NMP treatment group. Two hours after the SP mouse model was successfully established, the control group solely underwent PBS treatment. Conversely, the Dex treatment group and the UiO66-Dex@NMP treatment group were given atomized administrations of Dex and UiO66-Dex@NMP respectively (Dex dosage 1 mg/kg). Administration of atomized medication was conducted using the Atomization Drug Administration Apparatus for Rats and Mice (KW-DM-YWH, Nanjing Calvin Biotechnology Co., Ltd.), with a treatment duration of 25 minutes. Twenty-four hours post-treatment, blood was collected from the mice, and the sera from each group were subsequently frozen for the purpose of cytokines detection.

2.14 Pharmacodynamic Study

The levels of inflammatory cytokines TNF-α, IL-6 and IL-10 were measured according to the manufacturer's instructions of the respective kits. At the end of the treatment period, the mice were sacrificed by carbon dioxide asphyxiation, the lungs were isolated and processed for fixation, sectioning, and HE staining. The pathological scores of each group were then compared.

2.15 Statistical Methods

Data analysis was conducted using GraphPad Prism 6.0 software (GraphPad software, San Diego, CA, USA), with measurement data following a normal distribution described as mean $\pm$ standard deviation ($\bar{x} \pm$ s). Multiple group data differences were compared using repeated measures variance and one-way ANOVA analysis. Differences between the two groups were compared using two-way ANOVA analysis. When $p < 0.05$, it indicates that the difference is statistically significant.

3. Results and Discussion

3.1. Neutrophils Separation and Neutrophil Membrane Collection

Firstly, neutrophils were separated from bone marrow and peripheral blood. The isolated cells were conducted through Wright-Giemsa staining, revealed a distinct purple-

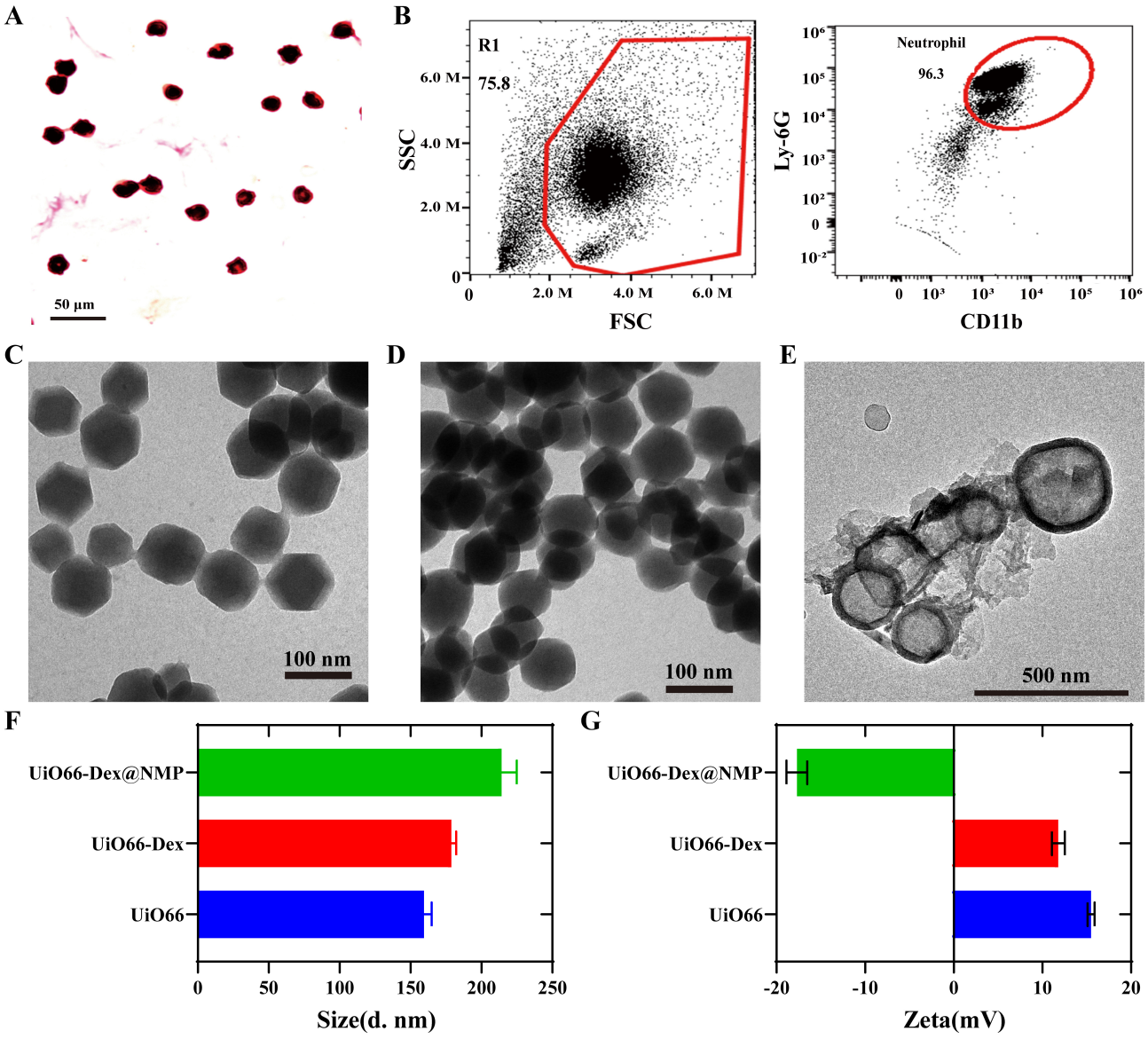

Fig. 2. Neutrophils separation and characterization of UiO66-Dex@NMP. (A) Wright Giemsa staining of the purified neutrophils. Scale bar = 50 μm. (B) CD11b biomarker analysis of the neutrophil by Flow cytometry. (C) Morphological observation of UiO66 by TEM. Scale bar = 100 μm. (D) Morphological observation of UiO66-Dex by TEM. Scale bar = 100 μm. (E) Morphological observation of UiO66-Dex@NMP by TEM. Scale bar = 500 μm. (F) Particle size analysis of UiO66, UiO66-Dex and UiO66-Dex@NMP. (G) Potentiometric analysis of UiO66, UiO66-Dex and UiO66-Dex@NMP. TEM, transmission electron microscope; FSC, forward scatter; SSC, side scatter.

blue lobulated nucleus, which is suggestive of the typical morphology associated with neutrophils, as clearly depicted in Fig. 2A. Neutrophils were preactivated by TNF-α, flow cytometry was employed to meticulously identify surface markers on the neutrophils. The findings presented in Fig. 2B illustrate that both Ly6G and CD11B positive cells accounting for 96.3% of the whole population. These observations strongly indicate that the neutrophils isolated in this study possess a remarkable degree of purity and a highly differentiated state.

3.2 Characterization of UiO66-Dex@NMP

The transmission electron microscopy (TEM) analyses of UiO66 and UiO66-Dex, depicted in Fig. 2C,D, unveil an average particle size of approximately 100 nm, displaying a distinctive octahedral morphology. The encapsulation of Dex had minimal impact on the particle size and morphology of UiO66-Dex, indicating that Dex is primarily adsorbed within the pores of UiO66-Dex. Fig. 2E showcases the TEM image of UiO66-Dex@NMP, featuring a typical core-shell structure adorned with a cellular membrane on its outer edge. This imagery provides compelling evidence of

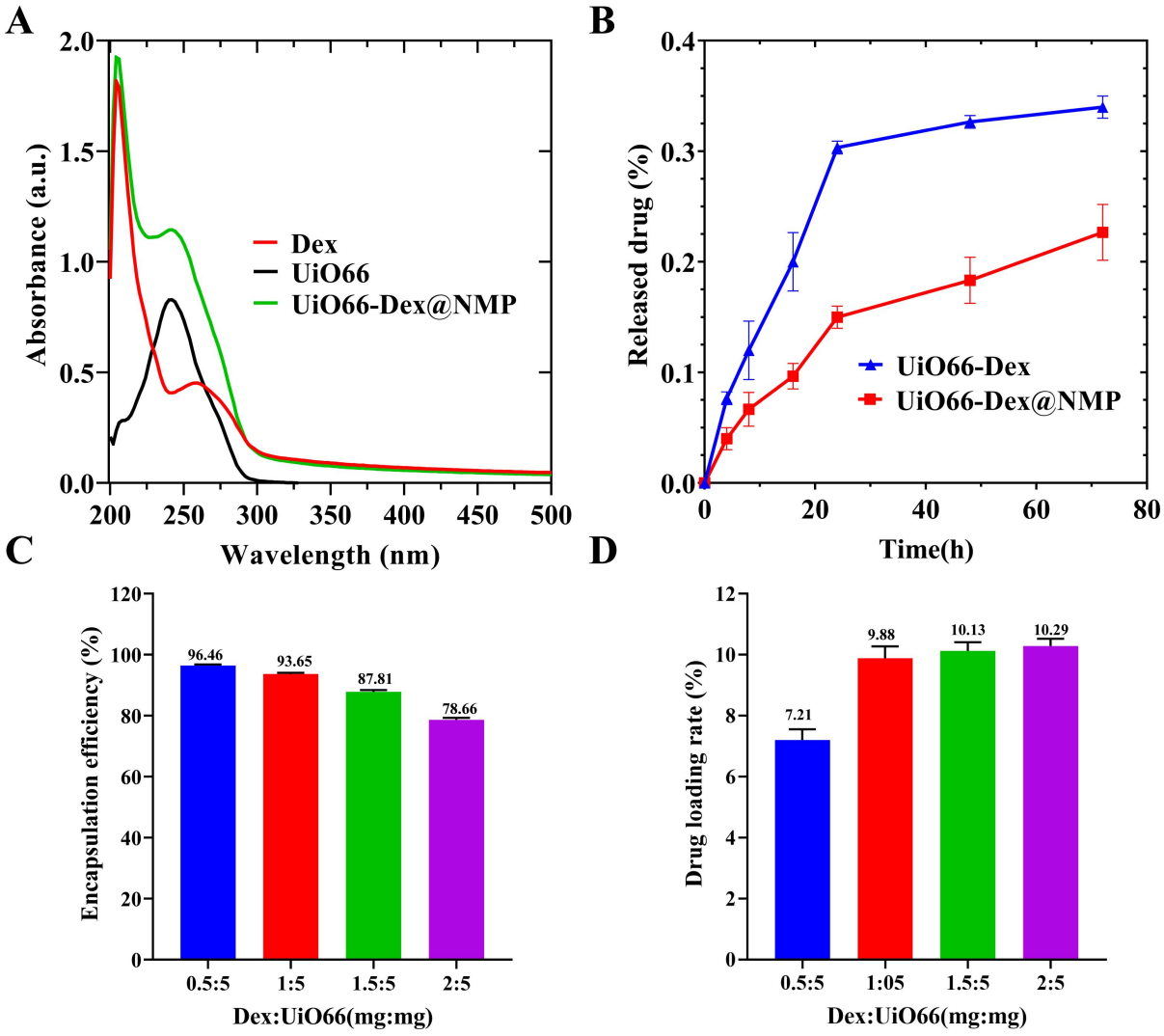

Fig. 3. Dex loading and release of UiO66-Dex@NMP. (A) Representative UV-visible absorption peaks of dexamethasone (Dex), UiO66-Dex, and UiO66-Dex@NMP in PBS. (B) *In vitro* release profile of UiO66-Dex@NMP in PBS over 72 hours. (C) Dex encapsulation rate test. (D) Dex loading test. UV, ultraviolet-visible.

the successful encapsulation of UiO66-Dex within the cellular membrane, with a mean particle size exceeding 100 nm. Fig. 2F presents the hydrated particle size data for UiO66, UiO66-Dex, and UiO66-Dex@NMP. The presence of a hydration film layer on the surfaces of these nanomaterials results in a measured hydrated particle size that is larger than the size observed through TEM. Furthermore, Fig. 2G illustrates the surface potential analysis of UiO66, UiO66-Dex, and UiO66-Dex@NMP. In aqueous solution, UiO66 and UiO66-Dex exhibit a positive charge, whereas UiO66-Dex@NMP carries a negative charge. This change in electric charge is attributed to the coating with neutrophil membranes.

3.3 Ultraviolet Absorption Spectrum of UiO66-Dex@NMP

To further characterize the structure of UiO66-Dex@NMP, the ultraviolet absorption was detected. As depicted in Fig. 3A, free Dex (curve in red), UiO66-Dex (curve in black) and UiO66-Dex@NMP (curve in green) all exhibit comparable absorption peaks at identical wavelengths at near 250 nm. Three different absorption curves demonstrate the successful encapsulation of Dex within UiO66-Dex@NMP.

3.4 Dex Loading Efficiency and Release Study

As shown in Fig. 3B, the cumulative release rates of Dex from UiO66-Dex and UiO66-Dex@NMP after 72 hours were 32.67% and 18.33%, respectively. Compared with UiO66-Dex, UiO66-Dex@NMP exhibited lower release rates at every time point, indicating that its release effect is more pronounced and sustained after undergoing biomimetic modification. This characteristic will effectively reduce unnecessary drug leakage and, in turn, lower the risk of side effects potentially caused by Dex. In

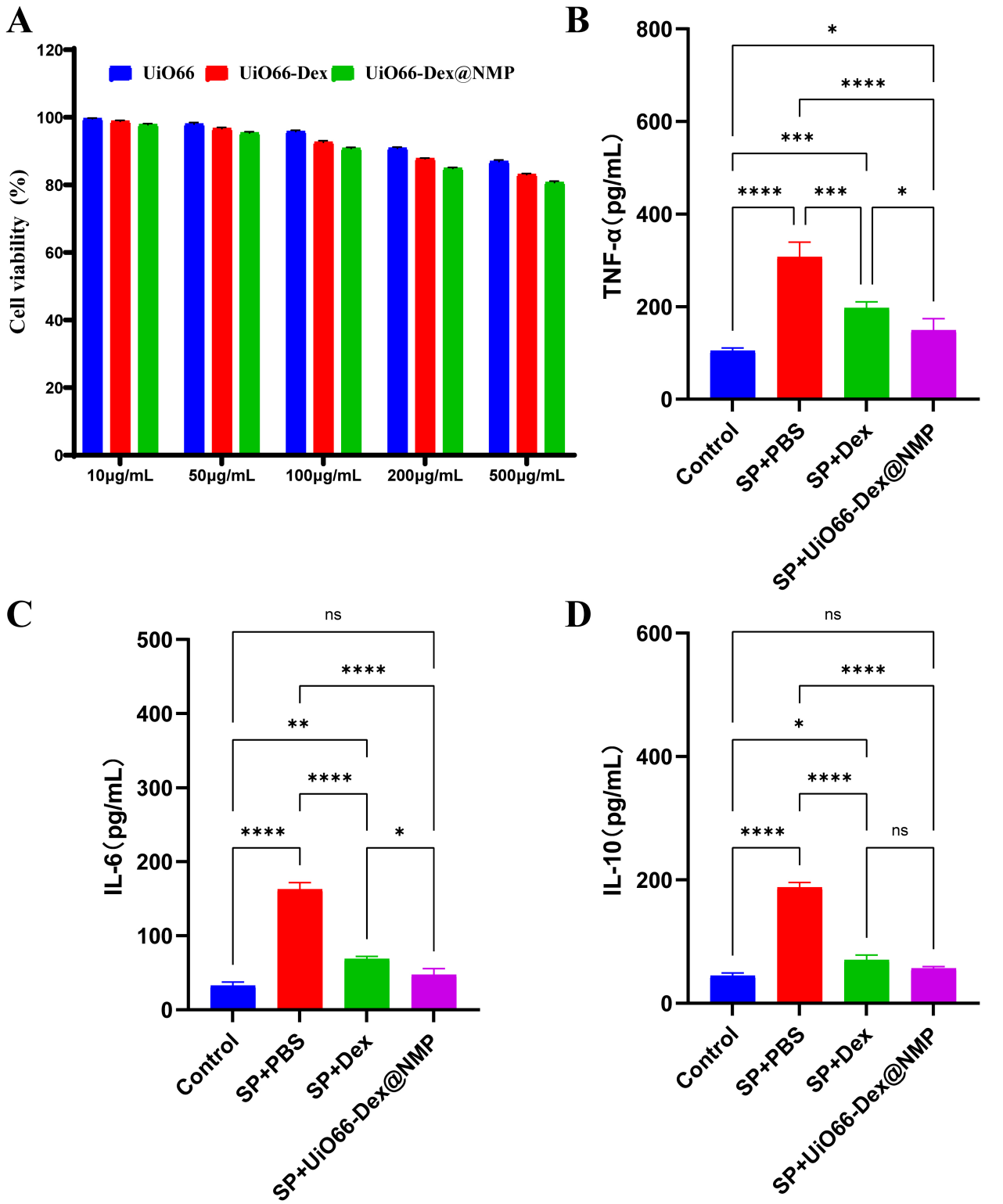

Fig. 4. Analysis of cellular toxicity and *in vitro* anti-inflammatory effects of UiO66-Dex@NMP. (A) RAW264.7 cytotoxicity assay. (B) RAW264.7 levels of the inflammatory factor TNF-α secreted by cells. (C) RAW264.7 levels of the inflammatory factor IL-6 secreted by cells. (D) RAW264.7 levels of the inflammatory factor IL-10 secreted by cells. TNF-α, tumor necrosis factor-α; IL-6, interleukin 6; SP, severe pneumonia. Statistical analysis was performed using two-tailed Student's *t*-tests. ns $p > 0.05$; * $p < 0.05$; ** $p < 0.01$; *** $p < 0.001$; **** $p < 0.0001$.

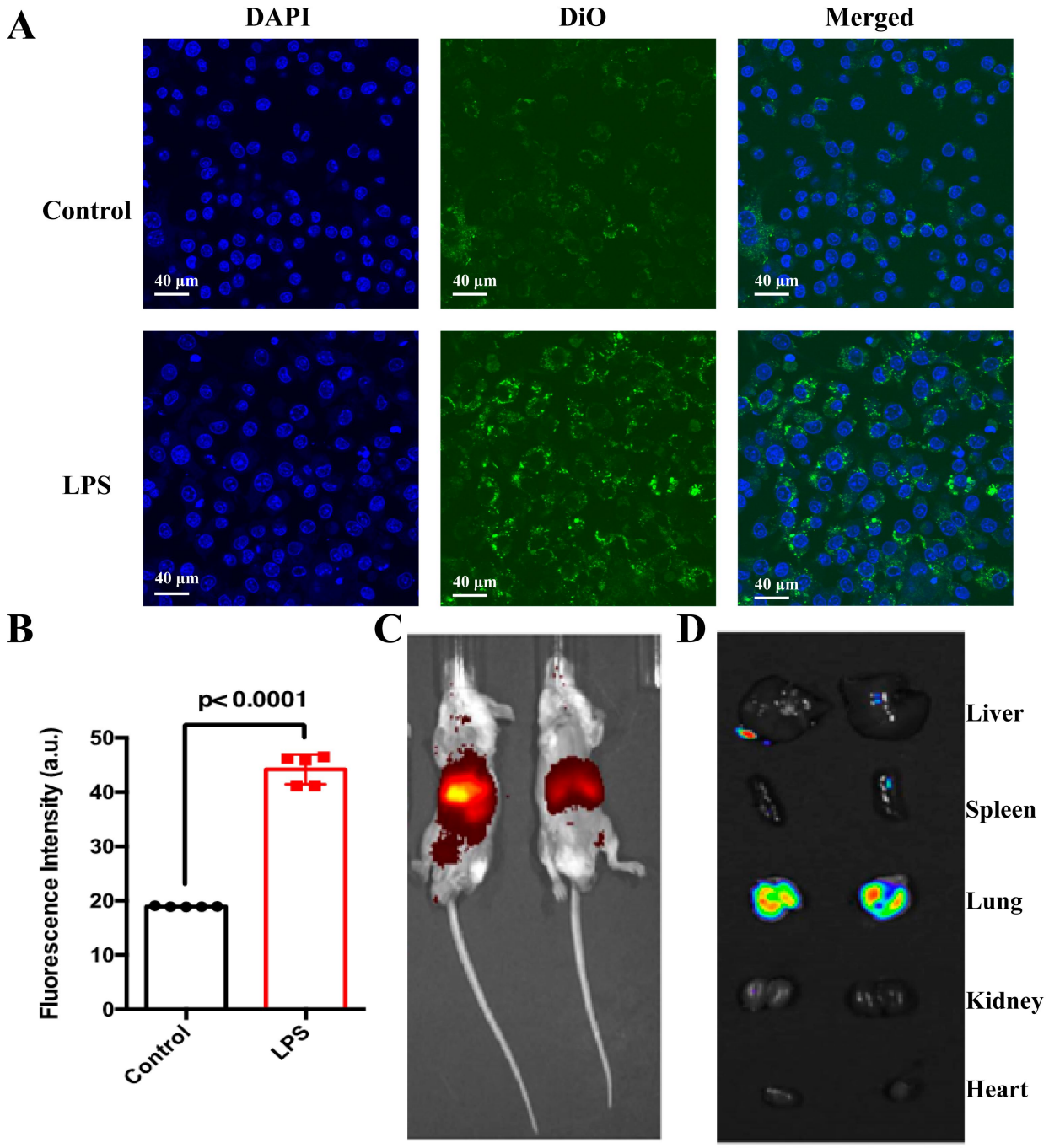

Fig. 5. ***In vitro*** **and** ***in vivo*** **targeting.** (A) Confocal fluorescence imaging of DiO-labeled NMPs after incubation with activated macrophages (blue, nuclei; green, UiO66-Dex@NMP). Scale bar = 40 μm. (B) Fluorescence quantification of UiO66-Dex@NMP per unit area on macrophages, $p < 0.001$. (C,D) *In vivo* targeting effect of DiR-labeled UiO66-Dex@NMP administered by atomization.

Fig. 3C,D, the optimum loading rate was achieved when the mass ratio of Dex to UiO66 was 1:5, and the Dex encapsulation rate at UiO66-Dex@NMP was 93.65 ± 2.74% with a drug loading of 9.88 ± 0.83%.

3.5 UiO66-Dex@NMP Cytotoxicity and Effects on Inflammatory Factors

As shown in Fig. 4A, at a concentration of 100 μg/mL or less, UiO66-Dex@NMP showed no significant toxicity to RAW264.7 cells, and the cell survival rates were all over 90%. The levels of inflammatory factors secreted by RAW264.7 cells were shown in Fig. 4B–D, and UiO66-Dex@NMP significantly reduced the TNF-α, IL-6, IL-10 levels. This indicated that UiO66-Dex@NMP had a significant inhibitory effect on the secretion levels of inflammatory factors.

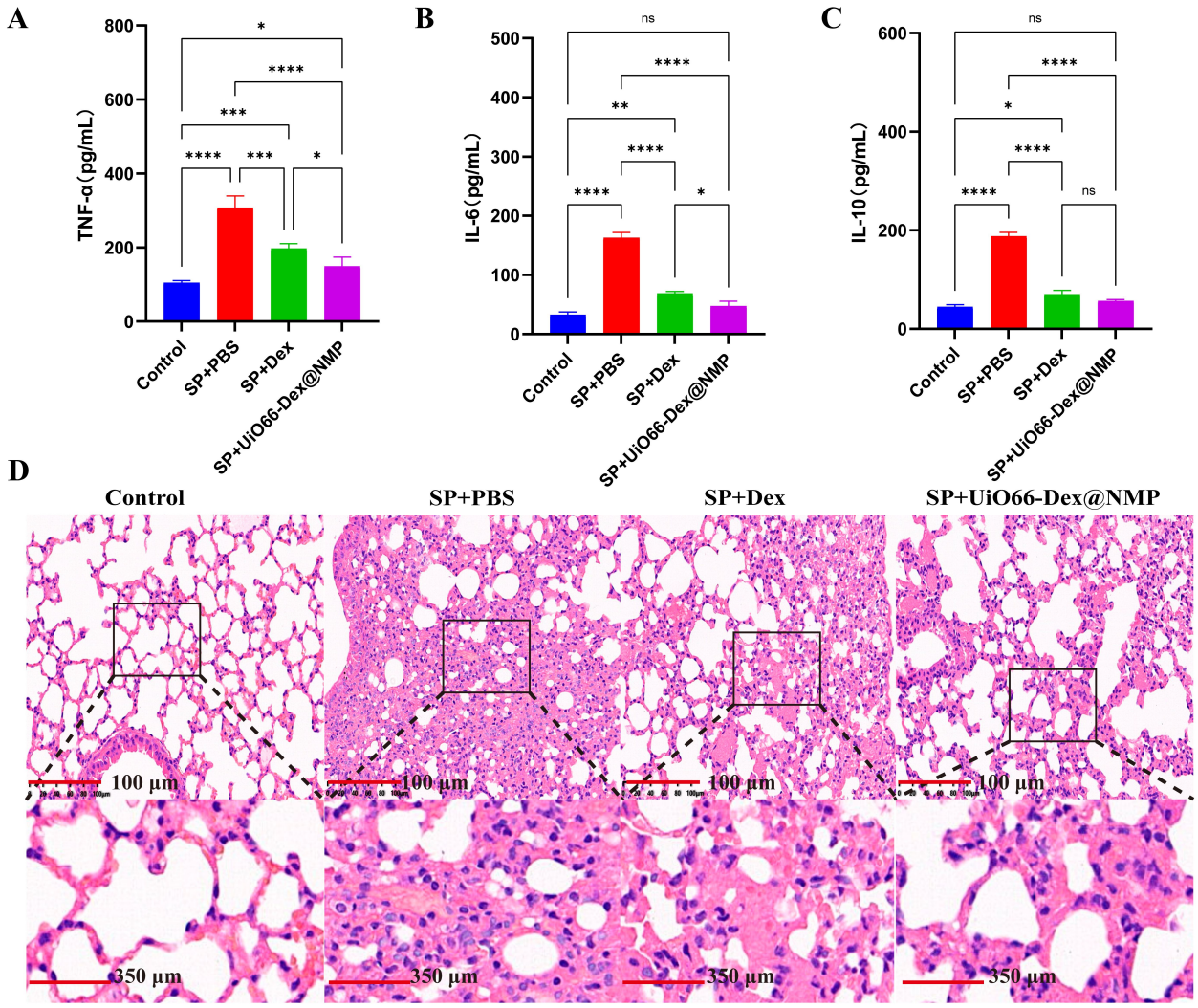

Fig. 6. Anti-severe pneumonia Therapy. The cytokines level after indicated treatments: (A) TNF-α; (B) IL-6; (C) IL-10; (D) HE–stained examination of lung tissues after indicated treatments. Scale bar = 100 μm (above); scale bar = 350 μm (below). Statistical analysis was performed using two-tailed Student's *t*-tests. ns $p > 0.05$; * $p < 0.05$; ** $p < 0.01$; *** $p < 0.001$; **** $p < 0.0001$.

3.6 In Vitro and in Vivo Targeting of UiO66-Dex@NMP

After UiO66-Dex@NMP was labeled with the cell membrane fluorescent dye DiO, it was co-incubated with mouse macrophage RAW264.7 cells and then observed under confocal microscopy. Fig. 5A demonstrates that RAW264.7 cells activated by LPS induction exhibited significantly increased green fluorescence compared to inactivated RAW264.7 cells (Fig. 5B). Consequently, UiO66-Dex@NMP displays a higher targeting efficiency towards activated macrophages in an inflammatory environment, thereby reducing the risk of nonspecific Dex delivery. As shown in Fig. 5C, the *in vivo* imaging of SP model mice after inhalation of DiR-labeled UiO66-Dex@NMP revealed that the fluorescent signal was primarily concentrated in the lungs. As depicted in Fig. 5D, indicated that apart from the lungs, there was no significant specific enhancement of fluorescent signals in other organs. Inhalation delivery further enhances the accumulation of therapeutic drugs in the lungs, thereby reducing unintended drug diffusion to other parts of the body.

3.7 Pharmacodynamic Study

Fig. 6A–C shows the serum cytokine levels in normal mice and SP model mice after receiving corresponding treatments. Compared to the normal control group, mice in the SP+PBS group exhibited significantly elevated serum levels of TNF-α, IL-6, and IL-10 (with extremely significant differences). However, after treatment with atomized Dex and UiO66-Dex@NMP, the serum levels of TNF-α, IL-6, and IL-10 in the mice were significantly reduced. Furthermore, compared to the mice treated with atomized Dex, those treated with UiO66-Dex@NMP showed significantly lower serum levels of TNF-α and IL-6, with a moderate reduction in IL-10 although the difference was not significant. Therefore, atomized UiO66-Dex@NMP treatment can sig-

nificantly reduce the levels of inflammatory cytokines in the serum of SP model mice, which may have a certain interventional effect on the inflammatory cytokine storm caused by SP. In addition, the neutrophil membrane has a certain adsorption effect on cytokines in the inflammatory environment, also known as "cytokine sponge" [15,23]. This is of great significance in reducing the inflammatory cytokine storm in SP. It is crucial to acknowledge that the influence of nanoparticles on inflammatory factors, including TNF-α, IL-6, and IL-10, may differ significantly both *in vitro* and *in vivo*, resulting in inconsistent effects across various experimental conditions and models.

The histological sections in Fig. 6D, revealed various degrees of pathological changes in the lung tissue of the SP model group. These included alveolar mice, collapse of alveolar walls, infiltration of inflammatory cells, dilation and congestion of capillaries, among other changes. In contrast, the lung tissue of the normal control group did not exhibit these changes, indicating the successful establishment of the SP model. When compared to the model group, both the Dex and UiO66-Dex@NMP inhalation treatment groups showed a reduction in the severity of SP-related pathological changes in the lung tissue. Furthermore, compared to inhaled Dex treatment, inhaled UiO66-Dex@NMP treatment further mitigated the pathological damage to the lungs caused by SP. Therefore, inhaled UiO66-Dex@NMP treatment demonstrated the most favorable therapeutic effect in SP, with significant improvements in both inflammatory cytokine levels and pathological lung injury.

4. Conclusions

UiO66-Dex@NMP exhibits remarkable targeting capabilities both in laboratory settings and in living organisms. To further investigate its potential, we conducted inhalation therapy studies using a mouse model of LPS-induced pneumonia. When compared to both the control group and dexamethasone sodium phosphate administered via inhalation, UiO66-Dex@NMP significantly decreased the degree of lung inflammation. Histopathological assessments confirmed that UiO66-Dex@NMP mitigated lung tissue damage. Consequently, UiO66-Dex@NMP emerges as a novel and safe carrier for inhaled dexamethasone delivery, providing significant insights into the clinical management of respiratory diseases, including severe pneumonia (SP). By harnessing the advantages of nano-formulation, atomized administration, and cell membrane-targeted delivery, this dexamethasone nanomedicine aims to reduce the overall dosage and systemic exposure of dexamethasone, thereby minimizing adverse side effects and enhancing patients' quality of life.

Availability of Data and Materials

The data and materials used in the current study are all available from the corresponding author upon reasonable request.

Author Contributions

KW and CX designed the research study. YY, HZ, and LY performed the research. YY, HZ, and LY analyzed the data and wrote the manuscript. YY edited the manuscript. All authors contributed to editorial changes in the manuscript. All authors read and approved the final manuscript. All authors have participated sufficiently in the work and agreed to be accountable for all aspects of the work.

Ethics Approval and Consent to Participate

The animal experiments conducted in this study complied with the relevant requirements of Laboratory Animal Welfare and Ethics Committee of Third Military Medical University (Approval No. AMUWEC20210417). The study was carried out in compliance with the ARRIVE guidelines.

Acknowledgment

We would like to express our sincere gratitude to the staff at the Laboratory Animal Center of the Third Military Medical University for their invaluable assistance in conducting the animal experiments.

Funding

This study was funded by the Cisen Pharmaceutical Public COVID-19 Scientific Research Fund (WPV01-CP-23).

Conflict of Interest

The authors declare no conflict of interest. Despite they received sponsorship from Cisen Pharmaceutical, the judgments in data interpretation and writing were not influenced by this relationship.

References

[1] de Benedictis FM, Kerem E, Chang AB, Colin AA, Zar HJ, Bush A. Complicated pneumonia in children. Lancet (London, England). 2020; 396: 786–798. https://doi.org/10.1016/S0140-6736(20)31550-6.

[2] Febbo J, Revels J, Ketai L. Viral Pneumonias. Infectious Disease Clinics of North America. 2024; 38: 163–182. https://doi.org/10.1016/j.idc.2023.12.009.

[3] Patel JM. Multisystem Inflammatory Syndrome in Children (MIS-C). Current Allergy and Asthma Reports. 2022; 22: 53–60. https://doi.org/10.1007/s11882-022-01031-4.

[4] Scott SJ, Pfotenhauer B, Weiner JJ, Hilleshiem J, Khubbar M, Bhattacharyya S. Respiratory Pathogen Coinfections in SARS-CoV-2-Positive Patients in Southeastern Wisconsin: A Retrospective Analysis. Microbiology Spectrum. 2021; 9: e0083121. https://doi.org/10.1128/Spectrum.00831-21.

[5] Rueda ZV, Aguilar Y, Maya MA, López L, Restrepo A, Garcés C, *et al*. Etiology and the challenge of diagnostic testing of community-acquired pneumonia in children and adolescents. BMC Pediatrics. 2022; 22: 169. https://doi.org/10.1186/s12887-022-03235-z.

[6] Clementi N, Ghosh S, De Santis M, Castelli M, Criscuolo E,

Zanoni I, *et al*. Viral Respiratory Pathogens and Lung Injury. Clinical Microbiology Reviews. 2021; 34: e00103–e00120. https://doi.org/10.1128/CMR.00103-20.

[7] Al-Kuraishy HM, Al-Gareeb AI, Mostafa-Hedeab G, Kasozi KI, Zirintunda G, Aslam A, *et al*. Effects of β-Blockers on the Sympathetic and Cytokines Storms in Covid-19. Frontiers in Immunology. 2021; 12: 749291. https://doi.org/10.3389/fimmu.2021.749291.

[8] Meidaninikjeh S, Sabouni N, Marzouni HZ, Bengar S, Khalili A, Jafari R. Monocytes and macrophages in COVID-19: Friends and foes. Life Sciences. 2021; 269: 119010. https://doi.org/10.1016/j.lfs.2020.119010.

[9] Attaway AH, Scheraga RG, Bhimraj A, Biehl M, Hatipoğlu U. Severe covid-19 pneumonia: pathogenesis and clinical management. BMJ (Clinical Research Ed.). 2021; 372: n436. https://doi.org/10.1136/bmj.n436.

[10] Kino T, Burd I, Segars JH. Dexamethasone for Severe COVID-19: How Does It Work at Cellular and Molecular Levels? International Journal of Molecular Sciences. 2021; 22: 6764. https://doi.org/10.3390/ijms22136764.

[11] Namazi N. The effectiveness of dexamethasone as a combination therapy for COVID-19. Acta Pharmaceutica (Zagreb, Croatia). 2022; 72: 345–358. https://doi.org/10.2478/acph-2022-0030.

[12] Wang C, Zhang Y, Dong Y. Lipid Nanoparticle-mRNA Formulations for Therapeutic Applications. Accounts of Chemical Research. 2021; 54: 4283–4293. https://doi.org/10.1021/acs.accounts.1c00550.

[13] Boson B, Legros V, Zhou B, Siret E, Mathieu C, Cosset FL, *et al*. The SARS-CoV-2 envelope and membrane pro-teins modulate maturation and retention of the spike protein, allowing assembly of virus-like particles. The Journal of Biological Chemistry. 2021; 296: 100111. https://doi.org/10.1074/jbc.RA120.016175.

[14] Yang Y, Wang K, Pan Y, Rao L, Luo G. Engineered Cell Membrane-Derived Nanoparticles in Immune Modulation. Advanced Science (Weinheim, Baden-Wurttemberg, Germany). 2021; 8: e2102330. https://doi.org/10.1002/advs.202102330.

[15] Wang H, Liu H, Li J, Liu C, Chen H, Li J, *et al*. Cytokine nanosponges suppressing overactive macrophages and dampening systematic cytokine storm for the treatment of hemophagocytic lymphohistiocytosis. Bioactive Materials. 2022; 21: 531–546. https://doi.org/10.1016/j.bioactmat.2022.09.012.

[16] Sargazi S, Sheervalilou R, Rokni M, Shirvaliloo M, Shahraki O, Rezaei N. The role of autophagy in controlling SARS-CoV-2 infection: An overview on virophagy-mediated molecular drug targets. Cell Biology International. 2021; 45: 1599–1612. https://doi.org/10.1002/cbin.11609.

[17] Long J, Sun Y, Liu S, Yang S, Chen C, Zhang Z, *et al*. Targeting pyroptosis as a preventive and therapeutic ap-proach for stroke. Cell Death Discovery. 2023; 9: 155. https://doi.org/10.1038/s41420-023-01440-y.

[18] Cesta MC, Zippoli M, Marsiglia C, Gavioli EM, Cremonesi G, Khan A, *et al*. Neutrophil activation and neutrophil extracellular traps (NETs) in COVID-19 ARDS and immunothrombosis. European Journal of Immunology. 2023; 53: e2250010. https://doi.org/10.1002/eji.202250010.

[19] Wu MX, Yang YW. Metal-Organic Framework (MOF)-Based Drug/Cargo Delivery and Cancer Therapy. Advanced Mate-rials (Deerfield Beach, Fla.). 2017; 29: 10.1002/adma.201606134. https://doi.org/10.1002/adma.201606134.

[20] Liu X, Liang T, Zhang R, Ding Q, Wu S, Li C, *et al*. Iron-Based Metal-Organic Frameworks in Drug Delivery and Biomedicine. ACS Applied Materials & Interfaces. 2021; 13: 9643–9655. https://doi.org/10.1021/acsami.0c21486.

[21] Wang Y, Yan J, Wen N, Xiong H, Cai S, He Q, *et al*. Metal-organic frameworks for stimuli-responsive drug deliv-ery. Biomaterials. 2020; 230: 119619. https://doi.org/10.1016/j.biomaterials.2019.119619.

[22] Zhao K, Guo T, Wang C, Zhou Y, Xiong T, Wu L, *et al*. Glycoside scutellarin enhanced CD-MOF anchoring for laryngeal delivery. Acta Pharmaceutica Sinica. B. 2020; 10: 1709–1718. https://doi.org/10.1016/j.apsb.2020.04.015.

[23] Li S, Wang Q, Shen Y, Hassan M, Shen J, Jiang W, *et al*. Pseudoneutrophil Cytokine Sponges Disrupt Myeloid Expansion and Tumor Trafficking to Improve Cancer Immunotherapy. Nano Letters. 2020; 20: 242–251. https://doi.org/10.1021/acs.nanolett.9b03753.